A Spheroid Positron Emission Tomograph for Brain Imaging: A Feasibility Study

David C. Ficke, John T. Hood and Michel M. Ter-Pogossian
Division of Radiation Sciences, Mallinckrodt Institute of Radiology, Department of Chemistry, Washington University School of Medicine, St. Louis, Missouri

It has been long recognized that the primary advantage of imaging the brain with a positron emission tomograph using GSO scintillation detectors placed on a spheroid surface is the large solid angle of acceptance for annihilation radiation, which results in improved system sensitivity and image signal-to-noise ratio. In the present study, we investigated spheroid system geometry, detector design and contribution of scattered coincidences. **Methods:** Scintillation detector distribution on a spheroidal surface was investigated by approximating the surface by polygons. Finding a suitable crystal for this purpose led to the development of an experimental GSO block-type detector. The fraction of scattered coincidences was experimentally evaluated using phantoms and detector pairs in conjunction with a testing platform, and the relationship between scatter fraction and phantom volume was obtained. **Results:** Spheroid geometry was best implemented with a polyhedron consisting of a series of consecutive rings formed by trapezoids. An experimental block-type detector with 36 GSO scintillators and four 14-mm-diameter photomultiplier tubes, together with custom electronics, yielded a spatial resolution of 3.4 mm FWHM and an energy resolution of 18% FWHM. Using nearly "ideal" scintillation detectors with a 350-keV threshold, we found the scatter fraction to be 0.32 for a 20-cm uniform phantom, 0.22 for a 15-cm phantom and closely proportional to the square root of the phantom volume. **Conclusion:** For cerebral studies, a spheroid PET using GSO scintillators has several advantages: optimized geometry for sensitivity, a dead-time fivefold smaller than an equivalent BGO system, and appreciably better light output for improved energy resolution and detector identification. The construction of such a system is within the capabilities of present technology.

Key Words: PET; three-dimensional imaging; GSO; spherical geometry

J Nucl Med 1996; 37:1219–1225

In PET, the image-forming variable yielding the distribution of the positron-emitting nuclide is supplied by annihilation photons escaping from the subject under study. It is desirable to maximize the collection of these photons by the radiation detectors, and to do so it is best to provide a solid angle as close as possible to 4 pi steradians. Unfortunately, several difficulties impede this goal. Some are purely practical, such as the high cost of obtaining the many detectors required. Others are more fundamental, such as the increased fraction of scattered radiation. Because of these difficulties, in most state-of-the-art positron emission tomographs, the solid angle of acceptance of the photons emitted from the imaged object is limited by detector placement architecture and septa collimation, which minimizes the deleterious effects of radiation scattered in tissue. As a result, most PET systems subtend a relatively small solid angle for radiation collection, and a large percentage of the annihilation photons is lost to the examination.

Received Jun. 1, 1995; revision accepted Nov. 9, 1995.
For correspondence or reprints contact: David C. Ficke, PhD, Division of Radiation Sciences, Mallinckrodt Institute of Radiology, 510 S. Kingshighway, Box 8225, St. Louis, MO 63110.

Historical Development

The solid angle of acceptance of PET devices has been considerably improved through volume or three-dimensional imaging, whereby more coincidence lines are used without interslice septa. While this approach seems contrary to conventional wisdom in slice-oriented PET systems using septa collimation, it has been implemented for nearly 20 yr. In two very different early approaches, one group placed two gamma cameras in coincidence (*1*), and the other used high-energy physics instrumentation to place multiwire proportional chambers in coincidence (*2,3*). These systems, which suffered from increased scattered radiation, low sensitivity and modest count-rate capability, were not used extensively in PET imaging. Development of more conventional slice-oriented PET systems eventually resulted in most of today's devices. In these machines, however, slice sensitivity was near maximum and as resolution improved, practical problems with event-counting statistics arose. Several investigators (*4–6*) therefore proposed volumetric imaging PET systems, which promised greater sensitivity and a reconstructed resolution that approached detector intrinsic resolution. One system (*4*) used BGO detectors organized in a partial sphere but with annular collimation for scatter reduction. The other (*5,6*) used an open BGO cylinder that allowed all possible coincidence lines for image contribution. Others proposed a NaI(Tl) system for volumetric imaging (*7*). While these efforts produced many interesting and valuable simulation results and algorithms (*8–11*), none have proved practical. One group recently completed a volumetric imaging PET composed of a hexagonal array of NaI(Tl) planar detectors (*12*), and more recently a system using an annular NaI(Tl) detector (*13*). This approach, which is less expensive than slice-oriented devices, has excellent resolution and produces three-dimensional images. However, because of its thin, continuous detector, it is no more sensitive than conventional systems and suffers from high count-rate problems. Scatter contribution is minimized by a high-energy threshold. This is the only extensively used practical implementation of a PET camera specifically designed for three-dimensional data acquisition.

In 1989, two independent studies (*14,15*) showed that removing the slice septa from two different commercial systems operating in a volumetric imaging mode causes image improvement in a limited central region of the systems' axial extent and image degradation at its end regions. In 1990, a neuro-PET system with a retractable septa was developed (*16*), and this feature has become standard on commercial devices from Siemens and General Electric Medical Systems (*17,18*). The advantages and costs of increasing the solid angle of acceptance by omitting slice collimation have been reported (*19*) but

improved event detection is needed to realize the best benefits (*20*).

Objective

We therefore investigated the advantages and disadvantages of performing PET imaging of the human brain using radiation detectors distributed on a spheroid surface surrounding the patient's head. We sought to determine if this approach would increase system sensitivity and signal-to-noise ratio in the examination for a given dose of radiation delivered to the patient.

We focused on a PET device for brain imaging for several reasons. A large percentage of PET examinations are of the brain, and this is not likely to decrease. Some researchers are interested in applying cerebral PET to the examination of children, infants and even neonates. Because of the drastic limits on radiation exposure demanded for these patients, a gain in sensitivity for such examinations would be highly desirable. In addition, the human head is well suited for PET imaging with a spheroid distribution of radiation detectors. The cranial cavity is in many subjects approximately circumscribable by a sphere. Thus a distribution of radiation detectors about such an organ, equidistant from its surface, would be roughly spherical. From the standpoint of data sampling and volume reconstruction, this is desirable. Moreover, in a spheroid distribution of detectors around the brain, the attenuation experienced by annihilation photons emanating from the brain and traveling towards the detectors is nearly uniform. This is due to the favorable geometry and to the fact that except for minor perturbations from air-filled sinuses and varying bone thicknesses, the human brain, cranium and scalp exhibit nearly constant linear attenuation in all directions. This nearly isotropic distribution of scattered radiation is a highly useful feature in a PET-imaging device without septa, and a nearly constant contribution of scatter facilitates its subtraction. Finally, the human head's location with respect to the rest of the body facilitates a spheroid distribution of detectors, which is not the case in thoracic examinations.

MATERIALS AND METHODS

Spheroid Configuration

Implementing a spheroid PET device entails placing radiation detectors on a spheroid surface while maintaining a high packing fraction without imposing impractical demands on detector configuration. A high packing fraction requires detectors (or detector modules) with a polygonal cross-section. These demands suggest an architecture in which a mosaic of small scintillation detectors is optically coupled to a smaller number of photomultiplier tubes. Applying "Anger" decoding logic, the scintillation event is identified by a given crystal (*21*). A scintillation event's position in a crystal (or group of crystals) is identified by the distribution of signals generated by the event in a series of photomultiplier tubes interfaced to the crystal(s). This is the structure utilized successfully in most commercial PET devices (*22*).

The approximation of a spheroid by a polyhedron composed of polygons, by no means a trivial problem, has been addressed in the literature (*23*). This approximation is used in Buckminister Fuller's "geodesic domes" and in the design of soccer balls. Because this solution is not readily applicable to detector modules using Anger positioning logic, a more practical approach is a polyhedron consisting of a series of concentric rings formed by trapezoids (Fig. 1). The shape is gradually distorted, from a square at the "equator" to a trapezoid towards the "poles". Because the rings are not interlocked (as in geodesic geometry), they can be assembled in different numbers. The spheroid PET in Figure 1 has six rings, but

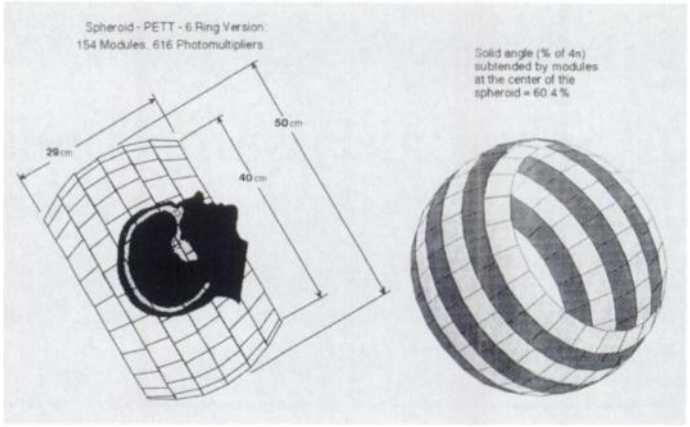

FIGURE 1. Diagram of a spheroid PET with six rings of trapezoid-shaped block detectors.

an eight-ring version is also practical. The detector surface area of the six-ring system is similar to that of the GE ADVANCE body system. However, it provides a solid angle of 7.5 steradians, compared to 2.2 steradians, for an advantage of 3.4; it has a 20% advantage in solid angle, compared to a cylinder with similar surface area; and it has a diameter that subtends a solid angle of 6.3 steradians. The architecture's complexity is in the variation of its trapezoidal cross-sections. In the illustrated design, there are three different shapes from the diagram in Figure 1 as shown in Figure 2. The distortion of the polygons from that of a square is not severe, and the same four 1-in. PMTs cover well the cross-section of even the "worst" polygon. The PMT with a 1-in. by 1-in. square cross-section was chosen to maximize light collection.

RESULTS

Experimental Investigation of Scattered Radiation

The large contribution of scattered radiation must be taken into account in designing detectors for spheroid geometry. Thus a preliminary effort in this investigation was constructing an apparatus (Fig. 3) that would provide a convenient platform for measuring the fractions of scattered and random coincidences in the proposed geometry. For a uniformly filled phantom, true and scattered coincidences are indistinguishable. By using substitution, however, two measurements may accomplish this purpose. The platform may be used with nearly "ideal" (highly efficient detection of all incident photons) detectors to restrict the measurements to reflect only source and field geometry influences, or used with more "realistic" detectors. For measurements with "ideal" detectors, two scintillation detectors operating in coincidence and incorporating cylindrical thallium activated sodium iodide crystals, 7.62 cm in diameter and 7.62 cm deep, each collimated by lead-tungsten to accept a circular

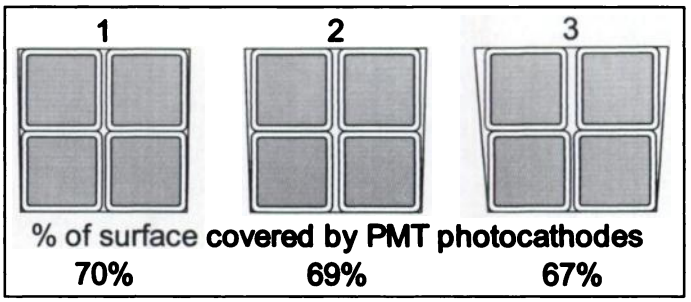

FIGURE 2. Trapezoid cross-sections of detector blocks for the six-ring spheroid PET shown in Figure 1. The distortion of the trapezoids from a square is not severe but does increase from the central rings (1 on left) to the outer rings (3 on right). The percentages shown represent the crystal mosaic portion covered by the photocathodes of the four 1-in. PMTs.

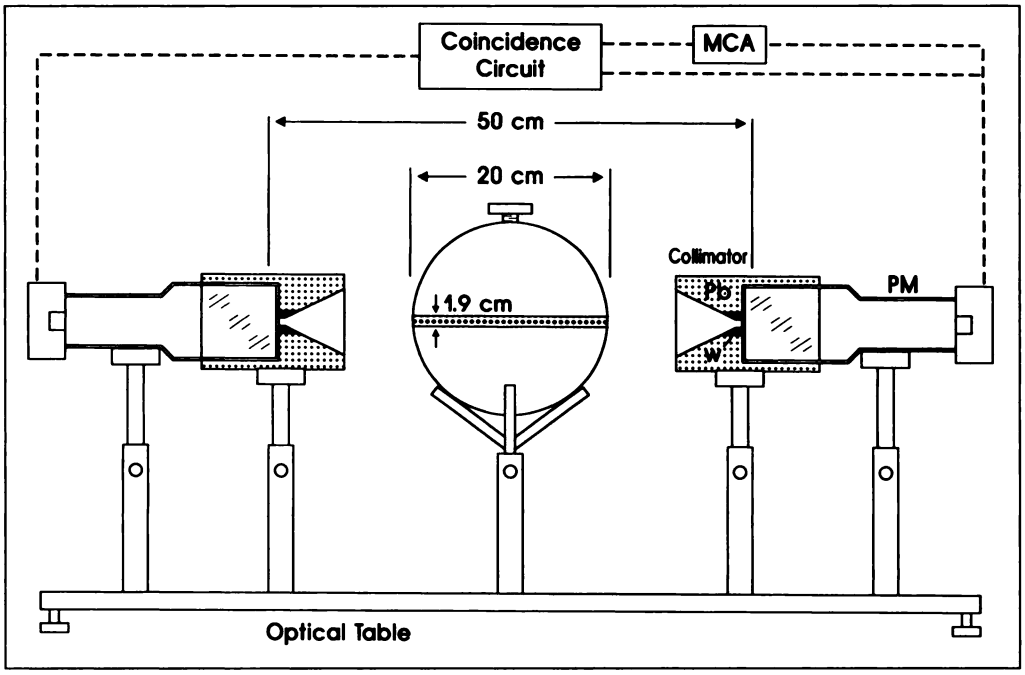

FIGURE 3. Diagram of the apparatus used for the experimental investigation of scattered radiation.

field of view 20 cm in diameter and 25 cm from the crystal surface were used. The aperture's diameter was 10 mm. The phantom was a plastic hollow sphere 20 cm in diameter containing a plastic cylinder with a 3.2-mm wall thickness and divided into two volumes: the sphere itself ("A") and a void in the sphere ("B") providing a cylindrical volume 19 mm in diameter. Volume "B" represented over 95% of the volume encompassed in the region where "true" coincidences could be recorded. Both volumes in the phantom could be filled with an aqueous solution or remain air filled. The volume of the 20-cm phantom though large for representing the human brain, was similar to the volume of the human head.

The system's electronics, interfaced to a workstation from Sun Microsystems Corp., were conventional. The apparatus in Figure 3 measured spatial resolution as a function of energy threshold, verified linearity as a function of energy and measured relative sensitivity as a function of energy.

Scatter and random coincidence contributions for the spherical phantom were measured at energy thresholds of 100, 250 and 350 keV for ^{18}F activity levels from 0.03–0.3 μCi/cc. Figure 4 shows spectra for the "true" and "scatter" counts at 0.03 μCi/cc. The true coincidence spectrum was collected with activity in the cylindrical insert and air in the surrounding sphere, while the scatter spectrum (with 8% randoms) was collected with water in the insert and activity in the surrounding sphere. Thus the detector pair could be used to measure the contribution of scattered coincidences in a uniformly filled sphere. The scatter fraction for the spectra was obtained by integrating all events after correction for sensitivity as a function of energy. Random coincidence contribution was calculated by $R = S \times S \times \sqrt{}$ Tal, where S is the measured single-photon counting rate and Tal is the 20-nsec coincidence window of the electronics.

The results in Table 1 provide an experimentally verified bound on scatter and random contribution that may be used to evaluate the feasibility of the spheroidal system. They reasonably agree with published experimental and analytically predicted results for cylindrical PET systems that use BGO block detectors and operate without septa (*14,15*). The scatter fraction S/(T + S) for a threshold of 350 keV is similar to findings in those reports and is likely due to the "ideal" detector design. But even in this case it should be noted that the sensitivity of the "trues" was effectively reduced by nearly a factor of two (from 14 to 7.5) because of noise contribution. The rapid increase of the scatter and random fractions for thresholds below 350 keV occurred because of the scatter's low energy contribution in the

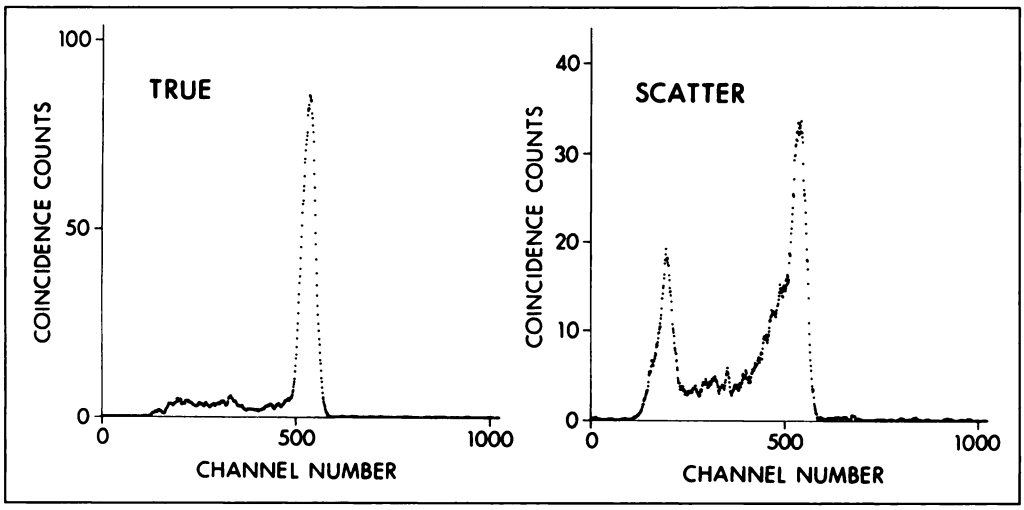

FIGURE 4. Spectra for true and scattered coincidences measured from a 20-cm spherical phantom at an ^{18}F activity level of 0.03 μCi/cc. The channel number was calibrated to energy in keV. The energy threshold was 100 keV.

TABLE 1
Count Performance at 0.3 μCi/cc Measured in a 20-cm Test Phantom

Et keV	T	S/T	S/(T+S)	R/T	Tne
100	19	1.02	0.50	0.98	6.3
250	15	0.66	0.40	0.69	6.4
350	14	0.47	0.32	0.40	7.5

T = true detector pair counts/sec/μCi/cc; S = scatter count rate; R = random count rate; Tne = T/(1 + S/T + R/T) = noise equivalent count rate.

spectrum (Fig. 4). Some randoms could be reduced by operating with a coincidence window narrower than the 20 nsec of the bench electronics, and substantial reductions could be obtained by using detectors with shorter decay times than BGO or NaI(Tl). It is important to note that, in terms of scatter and random contributions, scintillation detectors with densities similar to NaI(Tl) can operate with a performance similar to that of the much higher density BGO.

In addition to the collimated NaI(Tl) detectors used to establish best-case measurements, small detectors made with BGO, CsF or CsI, which might be more suitable for a spheroidal system, were used to measure scatter and random contributions. In these measurements 10-mm-diameter cylindrical crystal detector pairs were surrounded with a scattering medium similar both in density and effective atomic number to the scintillator tested. The purpose of this design was to include realistic detection in the scatter and random measurements, hence simulate the results that would be obtained in a system with closely packed small detectors.

BGO Block Detector

Because of its wide acceptance, BGO was tested first. The cylindrical scintillators (10 mm × 30 mm) were wrapped in a Teflon reflector enclosed in a thin aluminum housing. The annular container surrounding the detector was filled with granulated tungsten. At 511 keV, the measured spatial and energy resolutions of the detector pair were 5.0 mm FWHM and 18% FWHM, respectively. At 250 keV, measurements made with the 20-cm spherical phantom yielded a random contribution similar to that of the collimated NaI(Tl) detectors but a scatter contribution S/T of 0.99; at 350 keV, the S/T was 0.60. The performance of the BGO detectors operating independently underlines the significant contribution of edge effects to scatter fraction and suggests the need of a block detector to maintain a manageable scatter contribution.

In PET, the amount of scattered radiation reaching the detectors depends on the size and scattering characteristics of the structure imaged. This amount is mostly influenced by the size of the subject's head in brain studies. The 20-cm spherical phantom has a volume of over 4 liters and approximates that of the adult human head. As one of the stated objectives of the spheroid system is the imaging of infants and neonates heads, it was deemed important to assess the scattered radiation fraction as a function of head size. The ratio of scattered coincidences to true coincidences (S/T) was measured for two additional volumes with the above apparatus. The ratio plotted for three volumes (Fig. 5) was proportional to the square root of the volume. Thus, problems resulting from scattered radiation decrease rapidly with head size.

GSO Block Detector

The above measurements suggest that detectors suitable for a spheroidal PET system should be of a block design and should operate with an energy threshold of 350 keV or higher. The

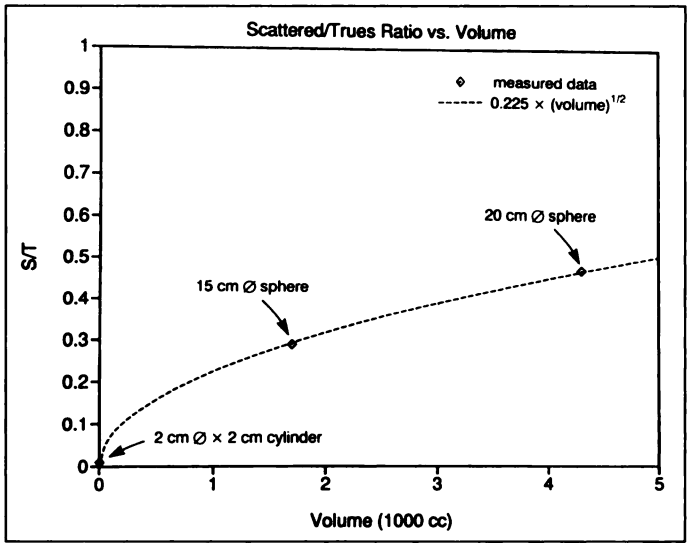

FIGURE 5. Measured ratios of scattered coincidences to true coincidences for three phantom sizes. The ratios were obtained using the apparatus shown in Figure 3 and are closely proportional to the square root of the phantom volume.

block detector minimizes edge effects, insures a high photopeak fraction of detected photons and when operated with a high energy threshold, effectively minimizes scattered coincidences for brain-size objects. In addition, the scintillator must have sufficient light output to accommodate photopeak acceptance above the threshold while rejecting scatter. High light output also facilitates the positioning system in the front-end electronics. Decay speed helps limit random coincidences and deadtime, and a high atomic number ultimately limits spatial resolution.

A scintillation material that exhibits many of the above properties for the spheroidal system is a crystal of cerium-activated gadolinium orthosilicate, GSO(Ce). This material has a density of 6.7 g/cc, greater light output than BGO, and a decay time of 56 nsec (*24*) (Table 2). In testing polished cylindrical crystals (10 mm × 30 mm) of BGO and GSO for light output, we observed that GSO had 2.9 times the effective light output of BGO and yielded an energy resolution of 11% FWHM at 511 keV (Fig. 6). LSO, a new scintillation crystal (*25*) that exhibits the most preferred characteristics of any known scintillator for this application, is not yet commercially available. Although our work has proceeded with GSO, it could easily be adapted to LSO if it becomes available. GSO was used with alternating crystals of BGO in a PET system developed by Scanditronix

TABLE 2
Physical Properties of BGO, GSO and LSO (*24–26*)

Property	BGO	GSO	LSO
Effective atomic number	75	59	66
Density (g/cc)	7.13	6.71	7.4
Decay constant (nsec)	300	56	40
Index of refraction	2.15	1.85	1.82
Peak wavelength (nm)	480	430	420
Attenuation length (cm)	1.12	1.38	1.14
Light yield (relative to NaI(Tl))	0.14*	0.41*	0.75
Hygroscopicity	No	No	No

*Based on measurements with same PMT and identical-size crystals of NaI, BGO and GSO. The BGO light yield varies in the literature with the BICRON Handbook of 1990 indicating 10%–20%. The GSO contains 0.5 mole% Ce doping.

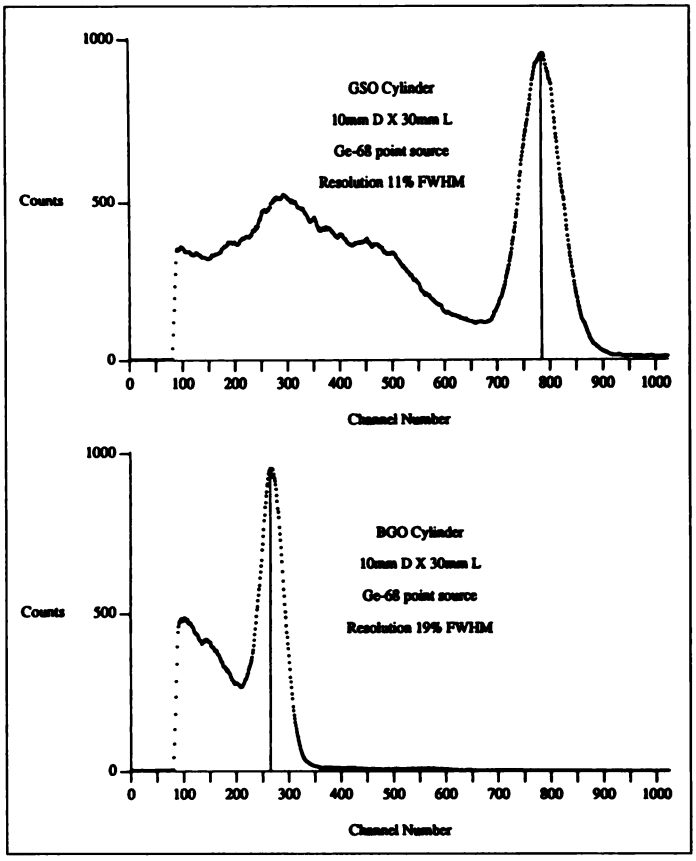

FIGURE 6. Energy spectra for polished crystals of GSO and BGO. The 511 keV peak energy channel is noted by the vertical line on each spectrum. The ratio of these channels indicates that the detected light output of GSO is 2.9 times that of BGO.

(*27*) but this effort was not continued, probably because of the high cost and manufacturing difficulties of GSO crystals at that time.

A block-type detector using GSO was designed and constructed as a square array of 36 diffusing surface crystals (4.5 × 4.5 × 30 mm) coupled to four 14-mm-diameter cylindrical photomultiplier tubes (Fig. 7). The module was tested under flood field and collimated beam illumination using single photons from a 511-keV radioactive source. Two sets of electronic instrumentation have been used: modularized bench instruments (*28*) and custom high-speed integrated circuits that digitize and record the four anode signals within 150 nsec of photon absorption. Because standard NIM electronics were designed for the slower decay of NaI(Tl) and BGO, the custom implementation was needed to demonstrate the ability to process events faster than the 750 nsec typically required for BGO. Software was developed to compute the two-dimensional Anger response and total energy response and to provide output in the form of plots and video images.

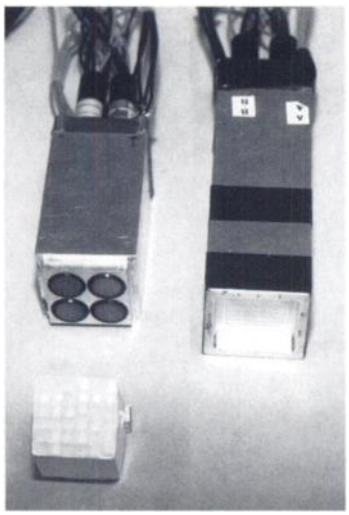

FIGURE 7. Experimental detector block with a 6 × 6 array of GSO crystals.

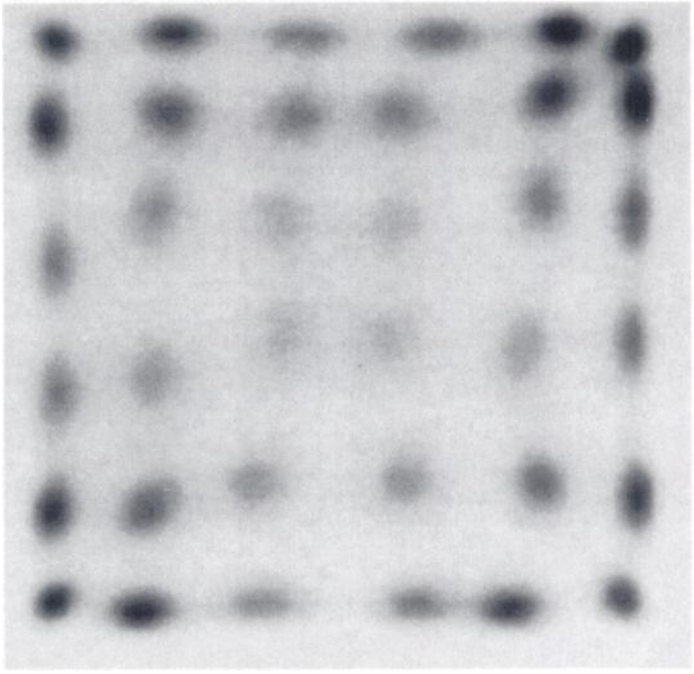

FIGURE 8. Two-dimensional Anger plot from the experimental detector block shown in Figure 7.

Results from the two electronic approaches were equivalent, demonstrating that the faster decay of GSO can be used by current technology to improve the count-rate capability and energy resolution of a block-type detector. Detectors arrayed 6 × 6 in a two-dimensional Anger plot (Fig. 8) were easily delineated, and an energy resolution of 18% FWHM was measured on a selected crystal. The detector block operated with 5 times less dead-time than a similar block of BGO (150 nsec instead of 750 nsec), which corresponds to the ratio of scintillation decay times. The lower stopping power, however, of GSO as compared to BGO resulted in an approximately 20% diminished sensitivity for 30-mm deep detectors. At higher activity levels the lower dead-time losses of the GSO helped preserve its sensitivity and the measured counting rate was greater than that for BGO.

Spatial resolution was measured for the block detector in coincidence with a detector identical to its individual component detectors. The line-spread function, obtained by stepping a 1-mm line source of ^{18}F at 0.5-mm increments across the field, was 3.4 mm FWHM. While no measurements were made for 4.5-mm BGO detectors, simulations (*29*) have shown their spatial resolution to be approximately 10% better than that of GSO.

The count rate of PET systems incorporating BGO block-type detectors is limited by their long decay time. At high-activity levels, the reconstructed spatial resolution of these devices may be degraded by inadequate counts, or they may require intolerably long data-acquisition times. Thus, at elevated counting rates, using GSO with a shorter decay time may yield an image with better spatial resolution.

To incorporate the block-detector design in the spheroid, a trapezoid rather than square cross-section must be accommodated. The difficulty in completely filling this shape with a

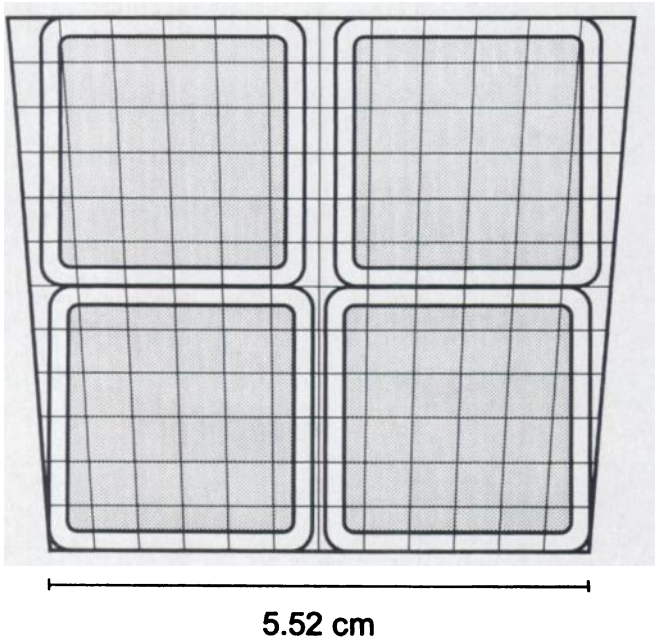

FIGURE 9. Illustration of a trapezoid detector showing the crystal mosaic.

mosaic of crystals can be overcome by cutting the crystals into suitable shapes to fill the trapezoids (Fig. 9). The individual crystals will vary somewhat in size and shape, but this is not a serious disadvantage since even rectangular modules have significant variations in spatial resolution, energy resolution and sensitivity (*30*). Because of their ability to maximize the collection of light from the GSO crystal block, the PMTs with square cross-sections achieve superior energy resolution for scatter rejection and for facilitating the positioning electronics to decode a large number of crystals. The Anger logic performs well even with some separation in the PMTs (Fig. 10).

DISCUSSION

Practical Considerations

Detector calibration and attenuation correction measurements for a spheroid PET are similar to those normally performed on cylindrical systems with a rotating rod source. In the case of the spheroid geometry, the rod is curved and a spheroid surface is traced.

Reconstruction and scatter correction algorithms for three-dimensional PET imaging are based on spherical geometry, for which, when used with cylindrical systems, the data must be transformed to spherical coordinates before processing. The spheroid PET offers a more natural geometry for these algorithms, although as in all PET systems, rebinning data into parallel projection planes is still required prior to algorithm implementation.

Data handling and computer implementation for a spheroid PET device are similar to that used at our institution in a previous system (*31*). A list-mode event acquisition system is used for maximum flexibility in data processing. For spheroid PET implementation, the bank-pair coincidence partitions are increased to 30 for improved count-rate performance, and the multiprocessor computer upgraded to 1 GFLOP of processing speed and 256 Mbyte of main memory capacity. This level of performance is available in many modern Unix-based servers and workstations. The cost of producing a spheroid PET device as described can be extrapolated with a good level of confidence from that of existing systems. The cost of components in a state-of-the-art body PET device having similar crystal surface area as the system of Figure 1 includes approximately 12% for the BGO scintillation crystals. At present, the cost of GSO is up to 2.5 times that of BGO, which increases the cost of the total system components by 19%. This estimate assumes reasonable consistency in the cost of other system components, such as electronics, gantry and patient support, and a computer system with peripherals.

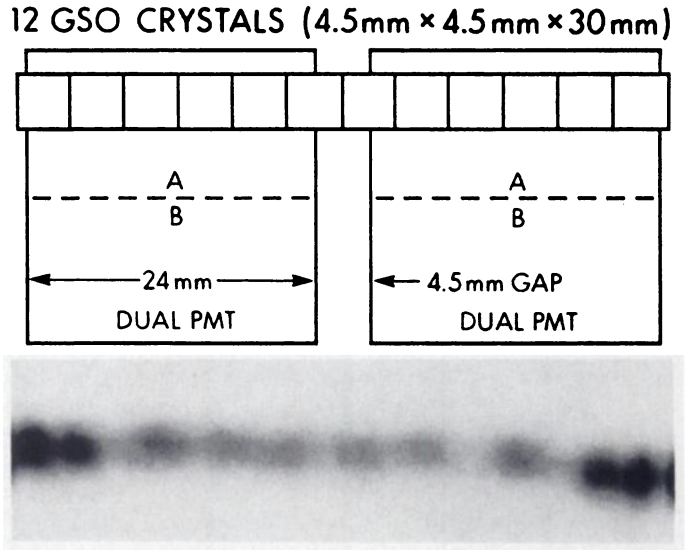

FIGURE 10. Experimental decoding of a linear array of 12 GSO crystals.

CONCLUSION

The study's findings indicate that a positron emission tomograph, designed for cerebral studies in which GSO scintillation detectors are distributed on a spheroid surface surrounding the subject's head has several advantages over more conventional devices:

1. The solid angle subtended by the detectors for a spheroid configuration is appreciably larger than that in conventional designs. Compared to a state-of-the-art body device, the spheroid geometry shown in Figure 1 subtends a solid angle approximately 3.4 times greater for about the same detector surface. Also, because of its more favorable angle of incidence for lines of measurement that are oblique to the transaxial plane, the spheroid configuration offers an improved axial-resolution variability.
2. The GSO mosaic radiation detector yields a dead-time approximately five times shorter than a BGO detector of the same size, which is of crucial importance in fast data-acquisition studies in which dead-time may result in serious information losses.
3. The GSO module described above provides an appreciably better energy resolution than a BGO module and therefore better scatter rejection. Its high light output facilitates the positioning electronics and allows a larger number of crystals to be decoded.

Conversely, a spheroid PET device utilizing GSO detectors exhibits several disadvantages as compared to conventional PET devices with BGO detector blocks:

1. The spheroid geometry does not lend itself to the use of interslice septa and must be operated only in the three-dimensional mode.
2. Because of its lower stopping power, the sensitivity of the GSO system is approximately 20% lower than a compa-

rable BGO system. The dead-time advantage of the GSO, however, results in less information loss and hence a higher true counting rate as activity levels increase.

3. Also because of its lower stopping power, the spatial resolution of the GSO system is approximately 10% poorer than a comparable BGO system with the same size crystals. To a certain degree this is offset by the more favorable angle of incidence of many lines of measurement in the spheroid configuration.

The cost of constructing a spheroid GSO PET is comparable to that of a more conventional design incorporating the same volume of crystal, except for the cost of GSO scintillation material, which is approximately 2.5 times greater than that of BGO. One can expect the overall component cost of the GSO device to be approximately 19% greater than that of a BGO system of comparable design. Experimentally, it has been shown that the magnitude of scattered coincidence contribution is manageable for cerebral studies, and algorithms for correction and reconstruction of three-dimensional images are available. From the engineering standpoint, the construction of a spheroid GSO PET for brain imaging is well within the capabilities of present-day technology.

ACKNOWLEDGMENTS

This work was supported by Department of Energy grant DE-FG02-93ER61522. We thank Thomas Lewellen and Robert Miyaoka from the University of Washington and David McDaniel from General Electric Medical Systems for useful discussions, assistance with measurements and sharing of equipment.

REFERENCES

1. Muehllehner G, Buchin MP, Dudek JH. Performance parameters of a positron imaging camera. *IEEE Trans Nucl Sci* 1976;23:528–537.
2. Jeavons AP, Townsend DW, Ford NL, Kull K, Manuel A, Fischer O. A high-resolution proportional chamber positron camera and its applications. *IEEE Trans Nucl Sci* 1978;25:164–173.
3. Jeavons A, Hood K, Herlin G, et al. The high-density avalanche chamber for positron emission tomography. *IEEE Trans Nucl Sci* 1983;30:640–645.
4. Cho ZH, Hong KS, Hilal SK. Spherical positron emission tomography (S-PET) I-performance analysis. *Nucl Instr Meth* 1984;A-225:422–438.
5. Burnham CA, Bradshaw J, Kaufman D, Chesler DA, Stearns CW, Brownell GL. Design of a cylindrical shaped scintillation camera for positron tomography. *IEEE Trans Nucl Sci* 1985;32:889–893.
6. Burnham CA, Kaufman DE, Chesler DA, Stearns CW, Wolfson DR, Brownell GL. Cylindrical PET detector design. *IEEE Trans Nucl Sci* 1988;35:675–679.
7. Rogers JG, Stazyk M, Harrop R, et al. Towards the design of a positron volume imaging camera. *IEEE Trans Nucl Sci* 1990;37:789–794.
8. Stearns CW, Burnham CA, Chesler DA, Brownell GL. Simulation studies for cylindrical positron tomography. *IEEE Trans Nucl Sci* 1988;35:708–711.
9. Stearns CW, Chesler DA, Brownell GL. Accelerated image reconstruction for a cylindrical positron tomograph using Fourier domain methods. *IEEE Trans Nucl Sci* 1990;37:773–777.
10. Kinahan PE, Rogers JG, Harrop R, Johnson RR. Three-dimensional image reconstruction in object space. *IEEE Trans Nucl Sci* 1988;35:635–638.
11. Kinahan PE, Rogers JG. Analytic three-dimensional image reconstruction using all detected events. *IEEE Trans Nucl Sci* 1989;36:964–968.
12. Muehllehner G, Karp JS, Mankoff DA, Beerbohm D, Ordonez CE. Design and performance of a new positron tomograph. *IEEE Trans Nucl Sci* 1988;35:670–674.
13. Freifelder R, Karp JS, Geagan M, Muehllehner G. Design and performance of the HEAD PENN-PET scanner. *IEEE Trans Nucl Sci* 1994;41:1436–1440.
14. Townsend DW, Spinks T, Jones T, et al. Three-dimensional reconstruction of PET data from a multiring camera. *IEEE Trans Nucl Sci* 1989;36:1056–1065.
15. Dahlbom M, Eriksson L, Rosenqvist G, Bohm C. A study of the possibility of using multislice PET systems for three-dimensional imaging. *IEEE Trans Nucl Sci* 1989;36:1066–1071.
16. Bailey DL, Jones T, Spinks TJ, Gilardi M-C, Townsend DW. Noise equivalent count measurements in a neuro-PET scanner with retractable septa. *Conference record of the IEEE NSS/MIC.* Arlington, VA. 1990;1217–1221.
17. Wienhard K, Dahlbom M, Eriksson L, et al. The ECAT EXACT HR: performance of a new high resolution positron scanner. *J Comput Assist Tomogr* 1994;18:110–118.
18. Degrado TR, Turkington TG, Williams JJ, Stearns CW, Hoffman JM, Coleman RE. Performance characterization of a whole-body PET scanner. *J Nucl Med* 1994;35:1398–1406.
19. Cherry SR, Dahlbom M, Hoffman EJ. Three-dimensional PET using a conventional multislice tomograph without septa. *J Comput Assist Tomogr* 1991;15:655–668.
20. Maze A, Lecomte R. Analytical study of the effect of collimation on the performance of PET cameras in three-dimensional imaging. *IEEE Trans Nucl Sci* 1990;37:823–831.
21. Anger HO. Scintillation Camera. *Rev Sci Instrum* 1958;27:29–33.
22. Casey ME, Nutt R. A multicrystal two dimensional BGO detector system for PET. *IEEE Trans Nucl Sci* 1986;33:460–463.
23. Williams RE. Handbook of structure. *Douglas Paper #5321.* Douglas Advanced Research Laboratories; 1968.
24. Takagi K, Fukazawa T. Cerium activated Gd_2SiO_5 single crystal scintillator. *Appl Phys Lett* 1983;42:43–45.
25. Melcher CL, Schweitzer JS. Cerium-doped lutetium oxyorthosilicate: fast, efficient new scintillator. *IEEE Trans Nucl Sci* 1992;39:502–505.
26. *BICRON Handbook.* Bicron Corporation; 1990.
27. Holte S, Ostertag H, Kesselberg M. A preliminary evaluation of a dual crystal positron camera. *J Comput Assist Tomogr* 1987;11:691–697.
28. Cutler PD, Hoffman EJ. Use of digital front-end electronics for optimization of a modular PET detector. *IEEE Trans Med Imag* 1994;12:408–418.
29. Ficke DC, Ter-Pogossian MM, Miyaoka RS, Lewellen TK. A GSO(Ce) block type detector for high count rate PET applications. *Conference record of the IEEE NSS/MIC.* Norfolk, VA. 1994;1859–1863.
30. Tornai MP, Germano G, Hoffman EJ. Positioning and energy response of PET block detectors with different light sharing schemes. *IEEE Trans Nucl Sci* 1994;41:1458–1463.
31. Ter-Pogossian MM, Ficke DC, Beecher DE, Hoffman GR, Bergmann SR. The Super PET 3000-E: a PET scanner designed for high count-rate cardiac applications. *J Comput Assist Tomogr* 1994;18:661–669.